Adenosine disphosphate–induced aggregation of human platelets in flow through tubes

I. Measurement of concentration and size of single platelets and aggregates

David N. Bell, Samira Spain, and Harry L. Goldsmith
McGill University Medical Clinic, Montreal General Hospital Research Institute, Montreal, Quebec H3G 1A4 Canada

ABSTRACT A double infusion flow system and particle sizing technique were developed to study the effect of time and shear rate on adenosine diphosphate–induced platelet aggregation in Poiseuille flow. Citrated platelet-rich plasma, PRP, and 2 μM ADP were simultaneously infused into a 40-μl cylindrical mixing chamber at a fixed flow ratio, PRP/ADP = 9:1. After rapid mixing by a rotating magnetic stirbar, the platelet suspension flowed through 1.19 or 0.76 mm i.d. polyethylene tubing for mean transit times, $\bar{t}$, from 0.1 to 86 s, over a range of mean tube shear rate, $\bar{G}$, from 41.9 to 1,000 s^{-1}. Known volumes of suspension were collected into 0.5% buffered glutaraldehyde, and all particles in the volume range $1–10^5$ μm^3 were counted and sized using a model ZM particle counter (Coulter Electronics Inc., Hialeah, FL) and a logarithmic amplifier. The decrease in the single platelet concentration served as an overall index of aggregation. The decrease in the total particle concentration was used to calculate the collision capture efficiency during the early stages of aggregation, and aggregate growth was followed by changes in the volume fraction of particles of successively increasing size. Preliminary results demonstrate that both collision efficiency and particle volume fraction reveal important aspects of the aggregation process not indicated by changes in the single platelet concentration alone.

INTRODUCTION

This work constitutes the second phase of an investigation into the effect of shear rate on the adenosine diphosphate–induced aggregation of human platelets in Poiseuille flow. In the first phase, ADP was directly infused into platelet-rich plasma, PRP, flowing through a 100-μm-diameter tube (Bell and Goldsmith, 1984; Bell et al., 1984). A microcinematographic technique permitted direct visualization of the aggregation reaction; however, the microscopic dimensions and constraints on the diffusion of ADP restricted its use to reaction times $\leq$27 s at mean tube shear rates >54 s^{-1}. The present technique circumvents the diffusion problem and extends the previous work to longer reaction times and higher shear rates. ADP and PRP are simultaneously infused into a common mixing chamber and, after a brief mixing period, flow through various lengths of polyethylene tubing into 0.5% glutaraldehyde. The effects of shear rate and transit time on platelet aggregation are followed through an analysis of the volume distribution of single platelets and aggregates from 1 to 10^5 μm^3. Suspensions such as PRP readily lend themselves to the application of two-body collision theory that can further characterize the effect of shear rate on agonist-induced platelet aggregation in Poiseuille flow. The present flow system also permits the use of higher molecular weight platelet agonists such as thrombin and collagen, and can be readily adapted for use with whole blood.

Platelet aggregation has been traditionally measured through the decrease in the optical density of stirred suspensions of platelets aggregating in response to an exogenous agonist (Born, 1962). Efforts to relate the concentration and size of aggregates to the optical density of the suspensions have shown that relatively small changes in suspension turbidity at early exposure times are accompanied by large decreases in the concentration of single platelets (Born and Hume, 1967), but that large decreases in turbidity later in time at high ADP concentrations are not necessarily associated with the further aggregation of single platelets (Gear and Lambrecht, 1981). Nichols and Bosmann (1979) measured the distribution of aggregate size and found that the relationship between particle concentration and optical density was nonlinear, and that in the presence of disaggregation the point of minimum optical density did not correlate with the point of maximum aggregate size. Chang and Robertson (1976) used an elaborate light scattering theory to follow the kinetics of aggregate growth in response to ADP at shear rates <75 s^{-1} in a cylindrical Couette, but found the light scattering phenomena to be dominated by single platelets, even after extensive aggregation. Gear (1982) used a resistive particle counter to measure the ADP-induced decrease in the concentration of single platelets in flow through tubes at mean shear rates <2,200 s^{-1}, but did not deal with the effect of shear rate on the kinetics of aggregate growth. Aggregate size distributions have been generated for shear-induced

platelet aggregation in cone and plate viscometers ($\geq$3,000 s^{-1}; Belval and Hellums, 1986; Belval et al., 1984) where it was observed that single platelets are still the most numerous particles at advanced stages of aggregation. In the lower physiological range of shear rate ($\leq$2,000 s^{-1}; Goldsmith and Turitto, 1986) of the present experiments, it is shown that aggregate growth is highly dependent on shear rate, and that changes in the concentration of single platelets do not reflect changes in aggregate growth.

In this paper, the flow system and particle counting and sizing procedure are introduced. A representative donor is used to illustrate the time course of ADP-induced aggregation over a range of mean tube shear rate from 41.9 to 1,000 s^{-1} through changes in the number concentration and volume of single platelets and aggregates. The fraction of collisions that result in the formation of stable aggregates, the collision efficiency, is determined from changes in the total particle concentrations according to classical two-body collision theory (Manley and Mason, 1952; Smoluchowski, 1917). Part II (Bell et al., 1989a) uses the technique and theory described herein to study the effects of shear rate, donor sex, and ADP concentration on the time course of ADP-induced platelet aggregation in suspensions flowing through tubes. Subsequent papers deal with the effect of ionized calcium concentration (Bell, D. N., S. Spain, and H. L. Goldsmith, submitted for publication) and red blood cells (Bell et al., 1989*b*).

GLOSSARY

Nomenclature

b	Sphere radius
D	Maximum absolute difference between $F^-(x_k)$ and $G(x_k)$ over all classes, $k = i$
D_{crit}	Maximum value of D beyond which $f^-(x_i)$ is not normally distributed, $P < 0.05$
D_t	Translational diffusion coefficient
E	Sum of squared error
$f(x_i); f^-(x_i)$	Measured platelet and aggregate log-volume histogram; minus background
f_m	Maximum class content of $f(x_i)$
$F(x_i); F^-(x_i)$	Normalized cumulative measured platelet and aggregate log-volume histogram; minus background
$g(x_i); G(x_i)$	Histogram of fitted Gaussian distribution to $f(x_i)$; normalized cumulative Gaussian histogram
$g_1; g_2$	Skewing; kurtosis of Gaussian distribution
G	Shear rate in uniform shear field
$G(R), G(R_0); \bar{G}$	Shear rate at radial distance R, value at wall; volume flow-averaged value in Poiseuille flow
H_0	Null hypothesis
i, k	Histogram class number
$j; j_c$	Two-body collision frequency; capture frequency
J	Total two-body collision frequency per unit volume of suspension
ℓ, u	Lower, upper histogram classes
L, U	Lower, upper volume of classes ℓ and u
$n(x_i), n_{L,U}$	Content of class i of any histogram, number of particles between L and U
$N; N_{L,U}, N_{L,U}(\bar{t})$	Number concentration of equal-sized spheres; between L and U, at time $\bar{t}$
$N_\infty(t)$	total particle concentration at time t
Pe	Péclet number
Q	Volume flow rate
r	Radius of curvature of coiled tube
$R; R_0$	Radial distance from tube axis; tube radius
Re	Tube Reynolds number
s, s^2	Standard deviation, variance of x_i
S	Suspension dilution factor
$t; \bar{t}$	Time, mean transit time
$U(R); \bar{U}$	Linear velocity in the axial direction at a radial distance R in Poiseuille flow; mean value
$v(x_i)$	Volume of class i
x	Limits of integration of normalized Gaussian density function corresponding to histogram classes
$x_i; \bar{x}$	Mark of class i of the log-volume histogram; mean value
X_3	Distance down flow tube from exit of chamber
Δx	Class width
$y(x_i), y'(x_i)$	Measured, fitted background log-volume histogram

Greek and script symbols

α, β, γ	Constants
α_0	Orthokinetic collision capture efficiency
η	Suspending fluid viscosity
$\bar{\mu}, \mu_{med}, \mu_{mod}$	Mean, median, mode of linear platelet volume distribution
ρ	Suspending fluid density
σ	Standard deviation of linear platelet volume distribution
$\Phi; \Phi(x_i), \Phi_{L,U}$	Particle volume fraction; of histogram class i, between L and U

MATERIALS AND METHODS

1. Platelet-rich plasma and reagents

Venous blood was slowly drawn from healthy volunteers via a 19-gauge needle and winged infusion set into 30-ml plastic syringes containing 1/10 volume, 3.8% sodium citrate. All donors had refrained from aspirin ingestion for at least 10 days before blood withdrawal and no female donors were taking oral contraceptives. After mixing by gently inverting the syringe, the blood was transferred to polycarbonate tubes and kept under a mixture of 95% air and 5% CO_2 to preserve pH 7.4. All subsequent platelet suspensions were maintained under this gas mixture.

The blood was incubated at 37°C for 30 min, centrifuged at room temperature at 100 *g* for 20 min, and the supernatant PRP containing from 3 to 5 $\times$ 10^5 cells μl^{-1} transferred to a 60-ml plastic Leur-Lok syringe. The suspension was diluted to 3.30 $\times$ 10^5 cells μl^{-1} with platelet-poor plasma, PPP, which was obtained by centrifuging the remaining blood at 2,000 *g* for 20 min.

Frozen aliquots of 2.0 mM adenosine-5′-diphosphate, ADP, (Sigma Chemical Co., St. Louis, MO) were thawed immediately before use and diluted in modified Tyrodes solution (137 mM NaCl, 2.7 mM KCl, 11.9 mM $NaHCO_3$, 0.36 mM $NaH_2PO_4 \cdot H_2O$) at pH 7.4. Electron microscopic grade glutaraldehyde (J. B. EM Services, Pointe Claire-Dorval,

Quebec) was diluted to 0.5% (vol/vol) in Isoton II (Coulter Electronics Inc., Hialeah, FL). 1% (vol/vol) silicone (Siliclad, Clay Adams, Parsippany, NJ) was used to siliconize the mixing chamber before experiments.

Monodisperse polystyrene latex spheres of 2.02, 5.00, 9.82, and 20.54 μm diameter (Coulter Electronics Inc.) were used to calibrate the particle sizing equipment.

2. Flow system and mixing chamber

All experiments were done at 23 ± 1°C. Platelet-rich plasma and ADP were simultaneously infused into a common mixing chamber (Fig. 1 *a*) by independent Harvard syringe pumps at a fixed flow ratio, PRP/ADP = 9:1 (Fig. 1 *b*). The infusion pumps responded linearly over the range of flow rates used to within ±1.1% and ±0.4% for the respective ADP and PRP flow rates. For flow rates ≥ 81 $\mu l\ s^{-1}$ it was necessary to use custom-made syringe pumps with motors of higher torque, reproducible to ±1.1% and ±2.6% for the ADP and PRP pumps, respectively.

The mixing chamber was constructed by placing a polyethylene-coated magnetic stirbar (4 mm length, 1 mm diameter) within a cylindrical section of polyethylene tubing (6 mm i.d., 9.5 mm o.d., 1.5 mm height), and sealing both between two glass slides. Platelet-rich plasma and ADP entered the chamber through five of six alternately located (3 PRP, 2 ADP) 18-gauge stainless steel tubes (20 mm length) spaced equidistant around the circumference of the mixing chamber. The rapidly mixed platelet suspension exited via the remaining stainless steel tube and flowed through 1.19 or 0.76 mm i.d. polyethylene tubing (Clay Adams), 2 cm–15.25 m long (16.8–12,800 tube diameters). Known volumes of the eluted platelet suspension were collected into 0.5% isotonic glutaraldehyde to give an ~20 times dilution of the plasma. The exact volume of the effluent was then determined by weight. Suspensions of fixed cells were maintained at room temperature with constant end-over-end rotation to prevent particle sedimentation until the concentrations were measured (≤2 d).

The length of time platelets spent in the mixing chamber was measured by injecting a 5-μl pulse of concentrated, glutaraldehyde-

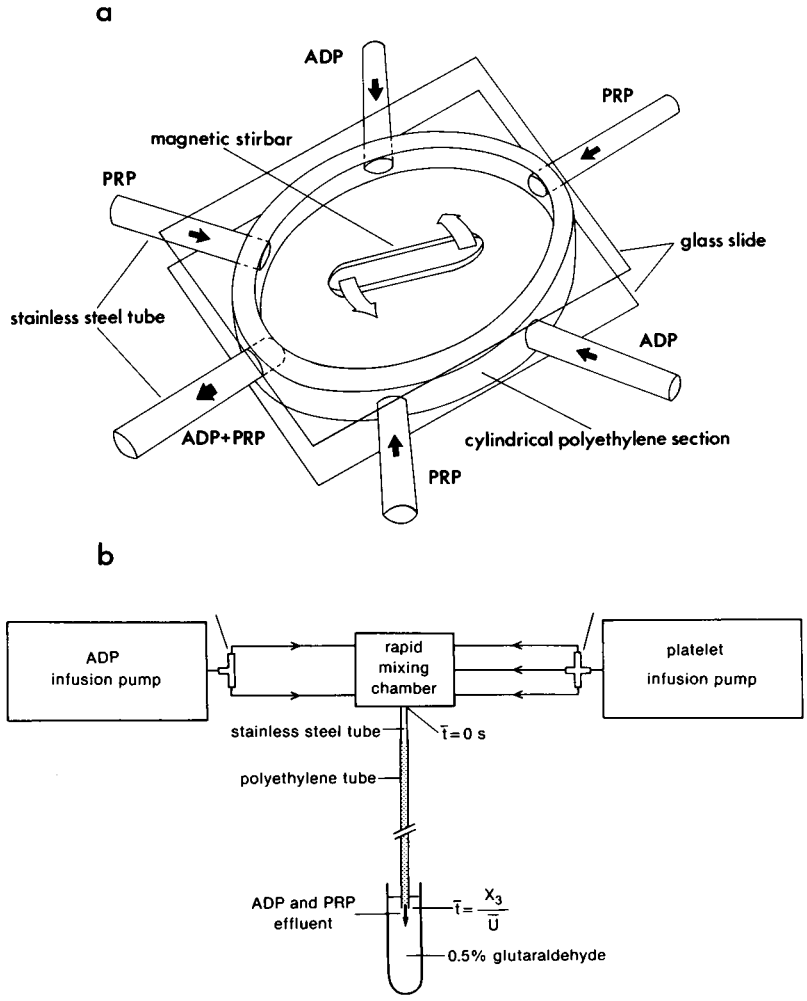

FIGURE 1 Flow system and mixing chamber. PRP and ADP are simultaneously infused into a common mixing chamber (*a*) by independent syringe pumps (*b*). After rapid mixing, the platelet suspension containing 0.2 μM ADP and 3.0×10^5 cells μl^{-1} flows through polyethylene tubes up to 15.25 m long. Known volumes of effluent are collected into 0.5% glutaraldehyde.

hardened platelets into the chamber through one entry port while diluent was pumped through the remaining entry ports at total volumetric flow rates corresponding to those used in the experiments. Measurement of the fraction of particles recovered from the chamber as a function of time after injection showed that only at flow rates $\leq 26\ \mu l\ s^{-1}$ did the residence time exceed 4 s. Above $52\ \mu l\ s^{-1}$, 50% of the particles had exited by 0.7 s, and 90% by 1.3 s. At the highest flow rate tested, essentially all particles had exited the chamber within 1 s after injection, which was the shortest sampling time feasible with the current technique.

Mean transit times of the platelet suspension through the flow tube, $\bar{t} = X_3/\bar{U}$, where X_3 is the distance down the flow tube and $\bar{U}$ is the mean linear fluid velocity, ranged from <0.1 to 86 s, depending on the volume flow rate, Q, and tube radius, R_0.

Volume flow rates of the platelet suspension through the flow tube were preset from 13 to $104\ \mu l\ s^{-1}$ (1.19 mm i.d.) and from 54 to $81\ \mu l\ s^{-1}$ (0.76 mm i.d.). If one assumes Poiseuille flow, the volume flow-averaged mean tube shear rate, defined as

$$\bar{G} = \frac{\int_0^{R_0} 2\pi U(R)G(R)RdR}{\int_0^{R_0} 2\pi U(R)RdR} \quad (1a)$$

$$= \frac{8}{15} G(R_0) = \frac{32Q}{15\pi R_0^3}, \quad (1b)$$

varied from 41.9 to $1{,}000\ s^{-1}$, inclusive, where $U(R)$ and $G(R)$ are the respective fluid velocity and shear rate at a radial distance R from the tube axis, and $G(R_0)$ the shear rate at the tube wall. Tube Reynolds numbers, $Re = 2R_0U\rho/\eta$, where ρ and η are the suspending phase density and viscosity, 1.02 g ml^{-1} and 1.8 mPa s respectively for human plasma at 22°C, were <80, thus ensuring laminar flow over the range of flow rates tested.

Tubes >1 m long were coiled vertically to prevent particle sedimentation within the flow tube. For all flow rates tested, the value of $Re\sqrt{R_0/r}$, where r is the radius of curvature of the coiled tube (400 mm), was below the critical value of $10^{1/2}$ at which secondary flow becomes significant (Schlichting, 1968).

3. Particle concentration and size measurement

The number and size of single platelets and aggregates were determined using an electronic particle counter (model ZM, Coulter Electronics Inc.). Voltage pulses corresponding to particle volume derived from the Coulter ZM preamplifier were amplified logarithmically (Coulter Logarithmic Range Expander) and then collated into a histogram of the logarithm of particle volume using a 100-channel, pulse-height analyzer (Coulter Channelyzer C1000).

Particles of volume $1–10^2\ \mu m^3$, corresponding to equivalent sphere diameter from 1.24 to 5.76 μm, were measured using a 50-μm-diameter × 60-μm-length aperture, and particles of volume $10^2–10^5\ \mu m^3$, corresponding to equivalent sphere diameter from 5.76 to 57.6 μm, were measured separately using a 100-μm-diameter × 120-μm-length aperture (Bell, 1988). The response of the instrument at the setting for the 50 × 60 μm aperture was tested over the range $1–10^2\ \mu m^3$ using 2.02-μm and 5.00-μm diameter calibration spheres and found to be perfectly logarithmic within a 6% error inherent in the assignment of a particle volume to a given channel of the pulse-height analyzer. The lower limit of the 100 × 120 μm aperture was matched to the upper limit of the 50 × 60 μm aperture using the 5.00-μm spheres. The 100 × 120 μm aperture was calibrated up to $4{,}540\ \mu m^3$ using 9.82- and 20.5-μm spheres. The expansion using this aperture was not perfectly logarithmic, however. Over and above the 6% assignment error, the measured modal volumes of the 9.82- and 20.5-μm-diameter spheres were 6.5 and 8% greater than the respective calculated mean volumes. The overestimation of the true particle volume appeared to increase with increasing particle size; however, because the instrument calibration was tested every 3 mo and found to remain constant throughout the duration of the experiments, all particles were measured under the same conditions.

Particle concentrations ≤ 14 and $\leq 4\ \mu l^{-1}$ were used in the 50 × 60 and 100 × 120 μm apertures, respectively, to prevent any concentration-dependent shifts in the volume distribution due to the slow response time of the d.c. restorer of the log range expander, and to keep particle coincidence to <10%. The suspensions of fixed cells were diluted in Isoton II electrolyte and counted for 100 s with the stopcock of the mercury manometer open, and the sample was continuously withdrawn to give total particle counts between 15,000 and 20,000, and between 5,000 and 40,000 on the 50 × 60 and 100 × 120 μm apertures, respectively. To avoid the sedimentation of the larger particles, the suspensions were continually stirred.

Multiple particle counts taken on the same sample dilution using each aperture were reproducible to ±2%. A 3% pipetting error in concert with this random counting error produced a maximum 5% variation in measured particle counts. After 4 d storage of the fixed platelet suspensions with constant mixing, there was no significant change in mean particle counts using either aperture. Thus, there was no particle aggregation or breakup induced by the fixation and storage procedure, as also shown previously for similar suspensions by Nichols and Bosmann (1979).

4. Log-volume histograms

Permanent tracings (Coulter XY4 Recorder) of the log-volume histograms were manually transposed into a microcomputer (model 86, Hewlett-Packard Co., Kirkland, Quebec) using a digitizer (HP 9111A). The upper limit of the last class of the histogram obtained using the 50 × 60 μm aperture was joined to the lower limit of the first class of the histogram obtained using the 100 × 120 μm aperture, to generate a single, continuous 250-class histogram over the range of log-volume from 0 to 5. The mark and the volume of the ith class are given by $x_i = (i - 0.5)\,\Delta x$ and $v(x_i) = 10^{x_i}$, respectively, where $\Delta x = 5/250$ is the class width. The generalized class content, $n(x_i)$, corresponds to either the number of particles in the ith class of the measured distribution of platelet and aggregate log-volume, $f(x_i)$, or that of the measured background distribution in glutaraldehyde-fixed PPP, $y(x_i)$. The number concentration per histogram class is given by $N(x_i) = Sn(x_i)$, where S is the suspension dilution factor.

The number of particles counted between the lower, $L = v(x_\ell)$, and upper $U = v(x_u)$, volumes corresponding to the lower, ℓ, and upper, u, histogram classes is given by:

$$n_{L,U} = \sum_{i=\ell}^{u} n(x_i), \quad (2)$$

and the number concentration by $N_{L,U} = Sn_{L,U}$.

The volume fraction of particles between L and U is given by:

$$\Phi_{L,U} = \sum_{i=\ell}^{u} \Phi(x_i), \quad (3)$$

where $\Phi(x_i) = N(x_i)v(x_i)$ is the volume fraction per histogram class.

All platelet distributions showed a pronounced negative skew (see Fig. 2) in the small volume range due to contaminating background in the glutaraldehyde-fixed plasma suspensions. Background was proportional to the concentration of fixed plasma in the electrolyte/cell suspension, and subtraction of $y(x_i)$ from $f(x_i)$ to yield the histogram

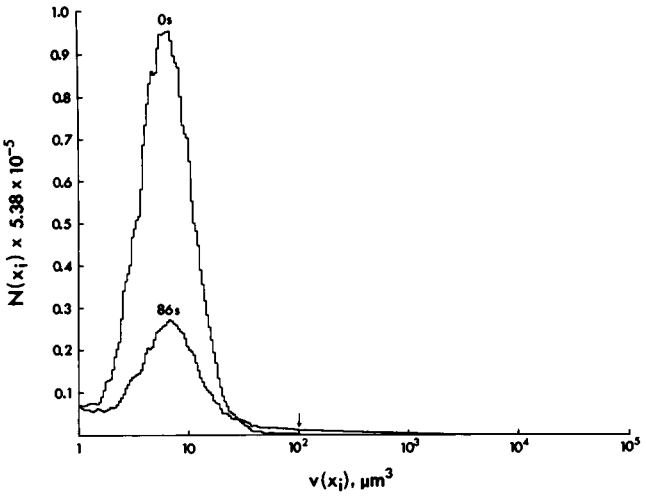

FIGURE 2 Log-volume histogram. The number concentration per histogram class $N(x_i)$ plotted against the equivalent sphere volume $v(x_i)$ over the range x_i = 0–5 for an unsheared control, $\bar{t}$ = 0 s, and after $\bar{t}$ = 86 s exposure to 0.2 μM ADP and $\bar{G}$ = 335 s^{-1}. Arrow at 100 μm^3 denotes point at which separate histograms from the 50 × 60 and 100 × 120 μm apertures were joined.

$f^-(x_i)$ at each mean transit time was facilitated by fitting an exponential curve to $y(x_i)$ and a normal curve to $f(x_i)$ at $\bar{t}$ = 0 s. Details of this procedure are given in the Appendix.

BASIC STATISTICS AND HYPOTHESIS TESTING

The mean, $\bar{\mu}$, standard deviation, σ, median, μ_{med}, and modal platelet volume, μ_{mod}, were calculated using the mean, $\bar{x}$, and variance, s^2, of the log-volume histograms, assuming a normal distribution of x_i (Bell, 1988) according to (Diem, 1962; Kenney and Keeping, 1951):

$$\log \bar{\mu} = \bar{x} + \frac{1}{2}s^2 \ln 10, \tag{4a}$$

$$\sigma^2 = \bar{\mu}^2(10^{s^2 \ln 10} - 1), \tag{4b}$$

$$\log \mu_{med} = \bar{x}, \tag{4c}$$

$$\log \mu_{mod} = \bar{x} - s^2 \ln 10. \tag{4d}$$

The assumption of log-normality of single platelet volume was tested using the Kolmogorov-Smirnov, K-S, one sample test (Young, 1977). The maximum absolute difference determined over all classes, $k = i$:

$$D = \max |F^-(x_k) - G(x_k)|, \qquad \ell \le k \le u \tag{5}$$

between the normalized cumulative log-volume histogram,

$$F^-(x_k) = \frac{\sum_{i=1}^{k} f^-(x_i)}{\sum_{i=1}^{u} f^-(x_i)}, \tag{6}$$

and the equivalent normalized Gaussian density function based on the sample statistics $\bar{x}$ and s^2,

$$G(x_k) = \int_{x=0}^{x-x_k+1/2\Delta x} \frac{1}{s\sqrt{2\pi}} e^{-(x-\bar{x})^2/2s^2}\, dx, \tag{7}$$

was compared to a critical maximum difference D_{crit}. The histogram class u, corresponding to the largest single platelet log-volume was determined by inspection of $f^-(x_i)$. The null hypothesis,

$$H_0\colon F^-(x_k) = G(x_k), \tag{8}$$

was rejected at the 5% significance level, and $f^-(x_i)$ was not considered to be normally distributed, if $D \ge D_{crit} = 0.886/\sqrt{\Sigma_{i=1}^{u} f^-(x_i)}$ (Lilliefors, 1967). Skewing, g_1, and kurtosis, g_2 of $f^-(x_i)$ and their standard errors were determined using standard equations for frequency distributions (Sokal and Rohlf, 1969). The significance of deviation of these sample statistics from the parametric value of zero was tested using two-tailed Student's t-tests. The above statistics were also applied to the single platelet region of $f(x_i)$ in which case $F(x_i)$ replaced $F^-(x_i)$ in the K-S test.

COLLISION FREQUENCY AND EFFICIENCY

The two-body collision frequency for monodisperse suspensions of rigid spheres in simple shear flow is given by (Manley and Mason, 1952; Smoluchowski, 1917):

$$j = \frac{32}{3} Gb^3 N, \tag{9}$$

where b is the sphere radius and N the number concentration. Collisions are defined as the rectilinear approach of sphere centers to within a distance of $\le 2b$, and provided $b/R_0 \ll 1$, Eq. 9 has been shown to apply in Poiseuille flow (Goldsmith and Mason, 1964). Using the mean tube shear rate, the total number of two-body collisions per second per unit volume of suspension is then:

$$J = \frac{1}{2} Nj = \frac{4\Phi \bar{G} N}{\pi}, \tag{10}$$

where Φ is the volume fraction of suspended particles.

Inclusion of the orthokinetic collision capture effi-

ciency, $\alpha_0 = j_c/j$ in Eq. 9, where j_c is the collision capture frequency, accounts for the influence of both interaction and hydrodynamic forces on particle capture (van de Ven and Mason, 1977). If $\alpha_0 = 1$, then $j_c = j$ and every collision results in capture; however, in the absence of attractive forces permanent capture is impossible (Brenner, 1961).

In the absence of aggregate break-up or the formation of higher order aggregates, the kinetics of aggregation are first order with respect to the total particle concentration, N_∞(Swift and Friedlander, 1964):

$$\frac{dN_\infty}{dt} = -\frac{4\Phi\alpha_0\bar{G}N_\infty}{\pi}. \quad (11)$$

Integration of Eq. 11 yields

$$\ln\frac{N_\infty(t)}{N_\infty(0)} = -\frac{4\Phi\alpha_0\bar{G}t}{\pi}, \quad (12)$$

where $N_\infty(0) = N$ and $N_\infty(t)$ are the total particle concentrations at time 0 and t, respectively. Thus, the total particle concentration decays exponentially and a plot of $\ln N_\infty(t)$ vs. t should give a straight line, the slope of which yields α_0.

In the present work the influence of Brownian motion on aggregation can be neglected due to the large value of the Péclet number, $Pe = \bar{G}b^2/D_t > 1{,}200$ where D_t is the translational diffusion coefficient for a single sphere calculated from the Stokes-Einstein equation. Thus, the measurement of the total particle concentration over the early stages of aggregation provides a value for α_0.

RESULTS

1. Single platelet distribution

a. Concentration and size

Before background subtraction, single platelet volume in unsheared suspensions appeared log-normally distributed (Fig. 2, $\bar{t} = 0$ s). Of a total 278,000 particles per microliter, >99% were in the range 1–30 μm^3, consisting principally of single platelets. Aside from the presence of some contaminating white blood cells of modal volume ~170 and 370 μm^3, measurements using the 100 × 120 μm aperture showed only ~0.06% of particles as aggregates >100 μm^3.

Shearing the suspension at $\bar{G} = 335\ s^{-1}$ in the presence of 0.2 μM ADP produced a time-dependent loss of single platelets accompanied by the formation of aggregates of successively increasing size (Fig. 2, $\bar{t} = 86$ s). Of the 98,000 particles per microliter remaining ~4% had volumes >100 μm^3, whereas >90% were in the volume range of single platelets. Thus, extensive aggregation involving as much as two-thirds of the original single cells reduced the fraction of singlets of the total number of particles by only 10%, and demonstrates the need for employing two apertures to count sufficient numbers of both single cells and aggregates in the same suspension. The accuracy of the sampling technique is evident by the continuity of the log-volume histogram in the region where the separate histograms from each aperture were joined (Fig. 2, *arrow*).

b. Curve fitting and background subtraction

The presence of contaminating background in the small volume region of fixed plasma suspensions interfered with the evaluation of the true shape of the distribution of single platelet log-volume (Fig. 2). The relative influence of background also increased as particle concentration decreased. Approximately 3% of particles counted as single platelets fell in the range 1–1.7 μm^3 at $\bar{t} = 0$ s, whereas at $\bar{t} = 86$ s this region accounted for 7.5% of the single platelets. Fig. 3 *a* shows the distribution of background in the autologous PPP of the platelet suspension shown in Fig. 2. Clearly this distribution is well matched to a decreasing exponential curve.

Fig. 3 *b* shows a normal curve initially fitted to the measured log-volume histogram at $\bar{t} = 0$ s over the region of the single platelet distribution where the influence of background and microaggregate contamination could be safely neglected (vertical arrows), and then afterwards extrapolated to include these regions of overlap. As shown by the ordinate, the background in PPP was less than that in PRP. Using the exponential curve, background was subtracted to give the same content in class 1 of the resultant histogram as that predicted by the normal curve (horizontal arrow). It is evident that after background subtraction the original normal curve closely fits the distribution of the logarithm of single platelet volume (Fig. 3 *c*). A proportionate amount of background was subtracted from the log-volume histograms at all subsequent mean transit times.

The Kolmogorov-Smirnov test strongly supported ($P < 0.05$) the assumption of log-normality of the distribution of single platelet volume and justified use of the fitted normal curve during background subtraction (Table 1, left). The presence of background produced a significant negative skewing ($g_1 < 0$) of the single platelet distribution which became significantly positive after ~4% of the total particles were subtracted as background. Positive skewing was more pronounced after background subtraction in the case of extensive aggregation (Table 1, right) where, as expected, the distribution of log-volumes was no longer normal. The deviation from log-normality was accompanied by an increase in mean and median volumes of this distribution. The mode remained con-

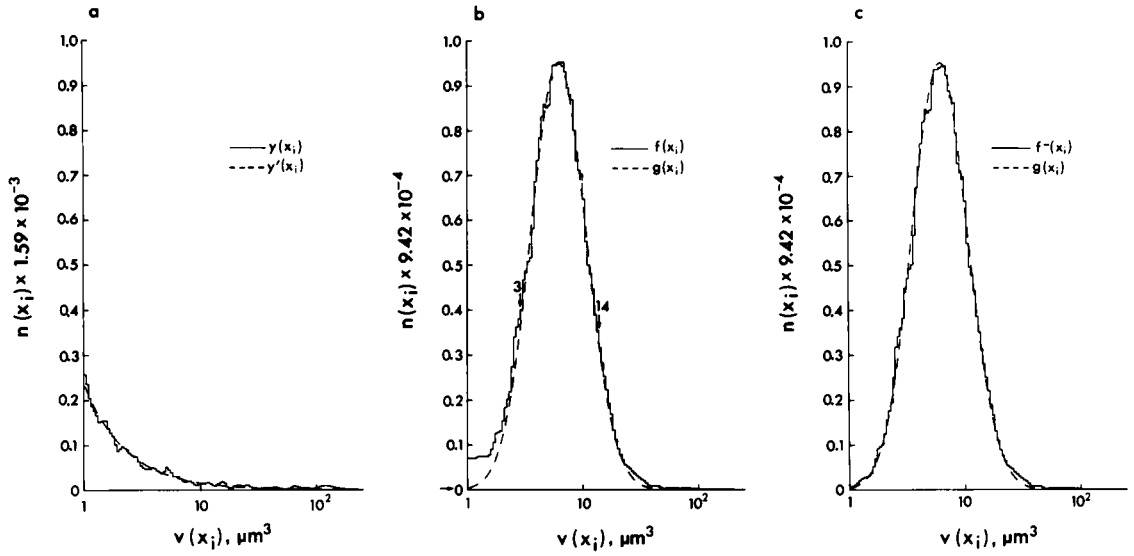

FIGURE 3 Curve fitting and background subtraction. (*a*) Exponential curve, $y'(x_i)$, (*dashed line*) fitted to the measured distribution of background, $y(x_i)$, (*solid line*) in the autologous PPP of the platelet suspension in Fig. 2. (*b*) Normal curve, $g(x_i)$, (*dashed line*) fitted to the measured single platelet distribution, $f(x_i)$, (*solid line*) over the range 3–14 μm^3 (*vertical arrows*). The fitted curve was then extrapolated in both directions to encompass the range 1–100 μm^3. Horizontal arrow denotes the frequency in class 1 of $g(x_i)$. (*c*) Background subtracted from each class of $f(x_i)$ over the range 1–10^5 μm^3 using $y'(x_i)$ to give the same content of particles in class 1 of the newly formed distribution, $f^-(x_i)$, (*solid line*) as that predicted by $g(x_i)$. The broken line shows $g(x_i)$ fitted to $f(x_i)$ before background subtraction.

stant, however, indicating that the removal of ~12% of the particles as background was valid.

2. Platelet aggregation

a. Single platelet concentration

One index of the degree of platelet aggregation is the time-dependent decrease in the concentration of single cells, $N_{1,30}(\bar{t})$, relative to the concentration $\bar{t}$ = 0 s. Fig. 4 shows the effect of mean tube shear rate on the normalized single platelet concentration. A noticeable 4-s lag preceded aggregation at all $\bar{G}$ tested. Aggregation then proceeded at rates dependent upon $\bar{G}$. At $\bar{G}$ = 1,000 s^{-1} the lag phase was so protracted that the initial rate of aggregation was much reduced, as was the final extent of aggregation reached at $\bar{t}$ = 86 s. The maximum rate and final extent of aggregation occurred at $\bar{G}$ = 168 s^{-1}. Above and below this shear rate, the degree of aggregation was always lower when measured by the decrease in the single platelet concentration.

b. Collision efficiency

Eq. 12 shows that the collision efficiency, α_0, is proportional to the slope of a plot of $-\ln[N_{1,10^5}(\bar{t})/N_{1,10^5}(0)]$ vs. $\bar{t}$, where $N_{1,10^5}(\bar{t})$ is the total measured particle concentration at time $\bar{t}$. Such plots are shown in Fig. 5 for the data in Fig. 4, and reveal a time and shear rate dependency for α_0 in the aggregating suspensions. Actual measurements of collision efficiency can only be made over the region of constant slope after the onset of aggregation. After the initial lag, α_0 remained relatively constant between $\bar{t}$ = 4

TABLE 1 Statistics of the single platelet distribution

Statistic	Control, $\bar{t}$ = 0 s		Aggregation, $\bar{t}$ = 86s	
	$f(x_i)$	$f^-(x_i)$	$f(x_i)$	$f^-(x_i)$
$\bar{x}$	0.78	0.80	0.79	0.85
s	0.27	0.25	0.34	0.29
$s/\bar{x}$ (%)	34.2	31.0	42.9	34.5
g_1	−0.14*	0.07*	−0.06*	0.22*
g_2	0.22*	0.08‡	−0.07‡	0.12‖
D	0.01550	0.00624‡	0.03096	0.02622
D_{crit}	0.00703	0.00718	0.00616	0.00656
$n_{1,85}$	15863	15213	20699	18214
$\bar{\mu}$	7.29	7.30	8.35	8.88
σ	4.83	4.50	7.63	6.74
$\sigma/\bar{\mu}$ (%)	67.2	61.6	91.4	75.9
μ_{med}	5.96	6.22	6.16	7.08
μ_{mod}	4.11	4.51	3.36	4.49

*P < 0.001. ‡Not significant. ‖P <0.05. ‖P < 0.002. Statistics of the single platelet log-volume and volume distributions summarized over the range 1–50 μm^3 for the data in Fig. 3 before $f(x_i)$ and after $f^-(x_i)$ background subtraction. Logarithmic data are shown in the upper part and after the appropriate linear transformation in the lower part for the unsheared control, $\bar{t}$ = 0 s (*left*) and after 86 s exposure to 0.2 μM ADP at $\bar{G}$ = 335 s^{-1} (*right*). Symbols are described in the text and volumes of the linear statistics are in cubed micrometers.

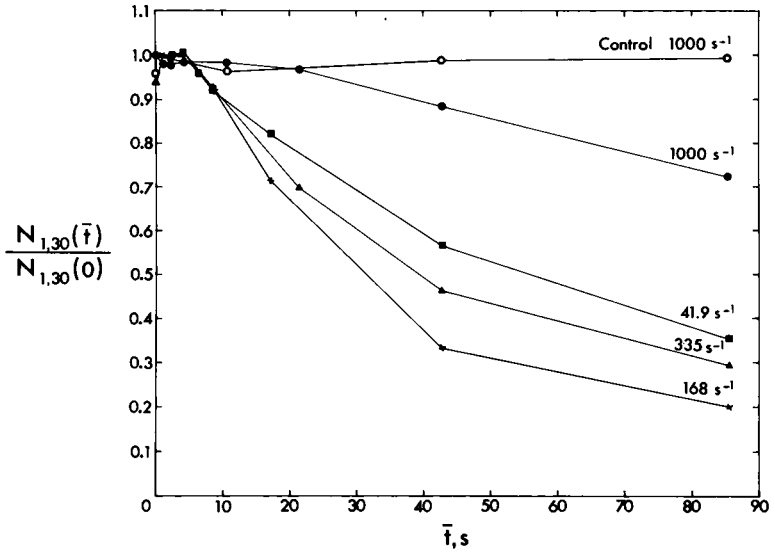

FIGURE 4 Single platelet concentration. The normalized single platelet concentration $N_{1,30}(\bar{t})/N_{1,30}(0)$, plotted against $\bar{t}$ for $\bar{G}$ = 41.9, 168, 335, and 1,000 s^{-1}.

and 43 s, but decreased with increasing $\bar{G}$ from $\alpha_0 = 0.098$ at $\bar{G} = 41.9\ s^{-1}$ to $\alpha_0 = 0.001$ at $\bar{G} = 1{,}000\ s^{-1}$. Beyond $\bar{t}$ = 43 s, α_0 appeared to decrease at all $\bar{G}$ below 1,000 s^{-1}.

c. Aggregate growth

As shown in Fig. 2, the number concentration of aggregates of volume >100 μm^3 was so low that frequency histograms do not adequately reflect the contribution of such particles to the total platelet concentration. As a result, the particle volume fraction per histogram class, $\Phi(x_i)$, was plotted against particle volume, $v(x_i)$, in Fig. 6 *a* for the same data as in Fig. 3 after background was subtracted. The relative contribution of large aggregates to the total volume fraction of cells is readily apparent. Fig. 6 *a* shows the formation of distinct peaks of aggregates of successively increasing size with increasing $\bar{t}$. A maximum aggregate size is also indicated by the sharp drop in particle volume fraction at 10^4 μm^3 at $\bar{t}$ = 86 s.

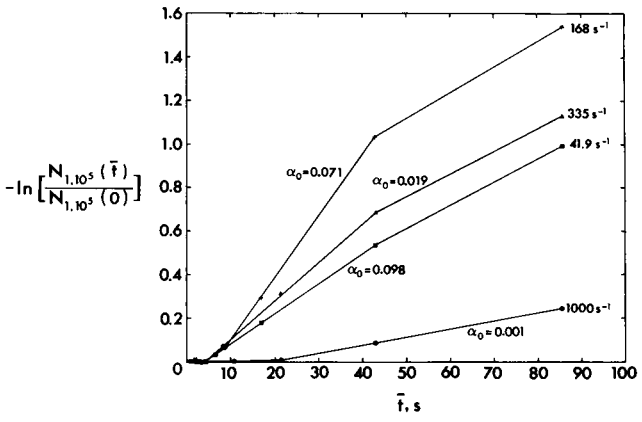

FIGURE 5 Collision efficiency. The negative logarithm of the normalized, total particle concentration, $-\ln [N_{1,10^5}(\bar{t})/N_{1,10^5}(0)]$, plotted against $\bar{t}$ for each of the four shear rates in Fig. 4. The values of α_0 were calculated over the range $\bar{t}$ = 4.3 to 43 s at $\bar{G} \leq 335\ s^{-1}$ and the range $\bar{t}$ = 21 to 43 s at $\bar{G}$ = 1,000 s^{-1} using Eq. 12.

The growth of aggregates of discrete size is illustrated in Fig. 6 *b* where the volume fraction of particles between lower, L, and upper, U, volume limits, $\Phi_{L,U}(\bar{t})$, normalized to the total volume fraction of particles at $\bar{t}$ = 0 s, $\Phi_{1,10^5}(0)$, is plotted against $\bar{t}$. The formation of aggregates of successively increasing size with increasing $\bar{t}$ is evident. The sharp drop in the fraction of particles corresponding to single platelets (1–30 μm^3) was accompanied by a successive rise and fall in the volume fraction of small aggregates from 30 to 10^2 μm^3. Aggregates between 10^2 and 10^3 μm^3 appeared later and only after $\bar{t}$ = 43 s did particles from 10^3–10^4 μm^3 appear. However, before the formation of aggregates from 10^3–10^4 μm^3, there was a rise in the fraction of particles from 10^4–10^5 μm^3 to ~30% which then decreased to ~3% by $\bar{t}$ = 86 s. This decrease was accompanied by both the appearance of aggregates from 10^3–10^4 μm^3 and a further rise in the volume fraction of particles from 10^2 to 10^3 μm^3, whereas the volume fraction of single platelets decreased only slightly. This pattern of aggregation suggests aggregate breakup at long $\bar{t}$. It should be noted that the total normalized volume fraction increased significantly above 1.0 with the appearance of aggregates >10^3 μm^3.

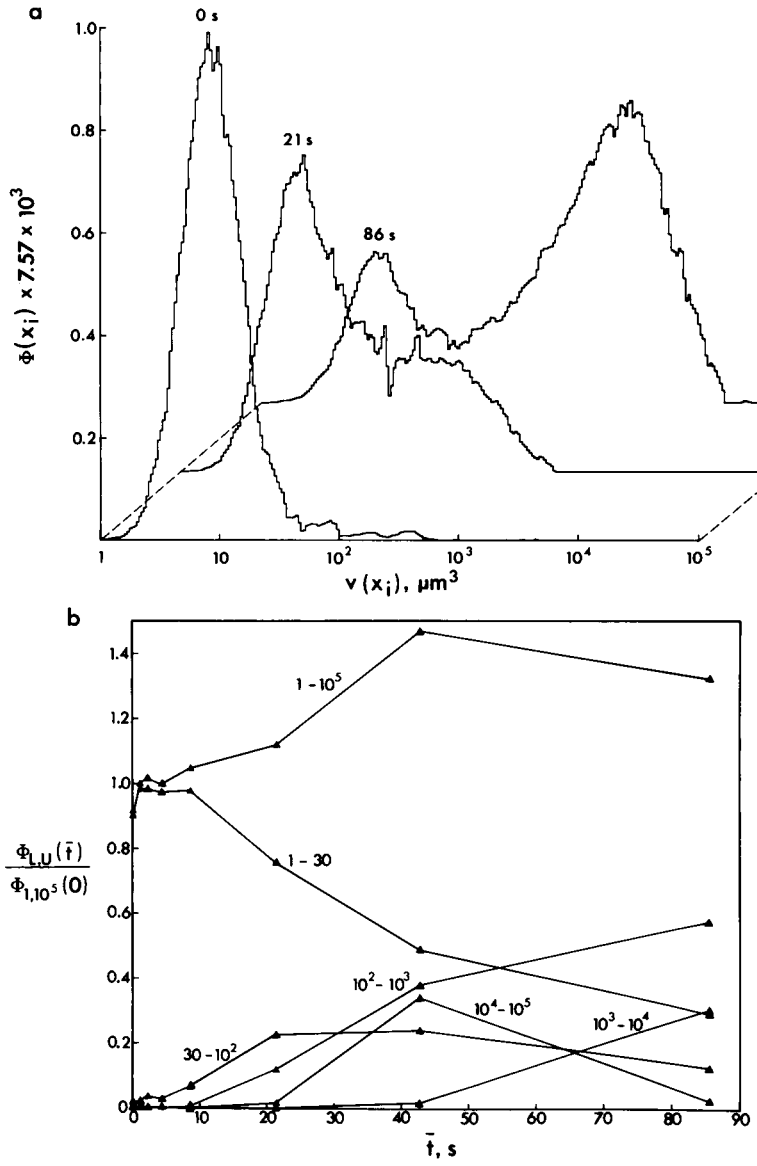

FIGURE 6 Aggregate growth. (*a*) Three-dimensional plot of the volume fraction per histogram class, $\Phi(x_i)$, vs. particle volume, $v(x_i)$ for the data of Fig. 2 at $\bar{t}$ = 0, 21, and 86 s after background subtraction. The time axis (*dashed line*) is not drawn to scale. (*b*) The normalized volume fraction of particles between lower, L, and upper, U, volume limits, $\Phi_{L,U}(\bar{t})/\Phi_{1,10^5}(0)$, plotted against $\bar{t}$ for the data of Fig. 2. The volume limits, L-U, from 1–30, 30–10^2, 10^2–10^3, 10^3–10^4, 10^4–10^5, and 1–10^5 μm^3 are shown beside their respective plots.

DISCUSSION

The present work has demonstrated the use of a flow system in which an aggregating agent is rapidly and uniformly introduced into a platelet suspension flowing through a tube, and which permitted platelet aggregation to be analyzed over a wide range of shear rate at both the early and late stages of the reaction. Particle counting and sizing instrumentation were configured to minimize errors inherent in their operation, and to allow the rapid measurement of the continuous volume distribution of single platelets and aggregates over the range 1–10^5 μm^3.

1. Single platelet volume

A dual aperture counting and sizing procedure was necessary to minimize sizing artifacts due to high particle-to-aperture diameter ratios (Smythe, 1961 and 1964). The dynamic working range of each aperture was

increased by using a logarithmic amplifier that allowed the continuous measurement of all single platelets and aggregates in the range of volume from 1 to 10^5 μm^3. A logarithmic expansion was also chosen because numerous studies have established a log-normal distribution of platelet size, whether determined by diameter, mass, or volume (Bahr and Zeitler, 1965; Paulus, 1975; von Behrens, 1972). The statistical analysis of the shape of the platelet log-volume distributions provided a sensitive measure of departures from normality and of the presence of microaggregates. The large variance in single platelet volume and the low number concentration of aggregates precluded the resolution of distinct peaks of microaggregates. From inspection of control platelet suspensions where the concentration of microaggregates was low, the range 1–30 μm^3 was selected to be principally single platelets, despite considerable overlap of single platelet and microaggregate volume. A more conservative estimate of the single platelet volume range, 1–50 μm^3, was selected for the statistical analysis of the single platelet volume distribution to reduce subjective bias in the selection of platelet volume.

Good agreement was found with the log-normal model for the distribution of single-platelet volume. The mean single platelet volume, after background subtraction, was found to be 7.3 μm^3 (Table 1). However, this value has to be corrected by a shape factor, defined as the ratio of the voltage pulse generated by a given particle to the minimum pulse height generated by a particle of the same volume. For an unactivated platelet, which rotates as a rigid oblate ellipsoid of revolution with a mean axis ratio of 0.36 (Frojmovic et al., 1976), the shape factor has been estimated to be 1.2 (Grover et al., 1969*a*; Velick and Goren, 1940). Because the Coulter ZM was calibrated with spheres of shape factor 1.5 (Gregg and Steidley, 1965; Grover et al., 1969*a* and *b*; Hurley, 1970), the measured volume of single cells and aggregates was that of the equivalent spherical particle. The measured single platelet volume must then be multiplied by 1.5/1.2 to give an absolute single platelet volume of 9.1 μm^3. The correction factor of 1.25 has been experimentally verified for the ratio of the volume of the approximately spherical platelets suspended in EDTA to the approximately discoid platelets in citrated plasma, and found to remain relatively constant after fixation of the cells in glutaraldehyde (Mundschenk et al., 1976). In addition, after exposure to 10 μM ADP, the volume of the more spherical shape-changed platelets was ~25% greater than the uncorrected volume of their unactivated, more discoid counterparts when measured on a Coulter Counter (Holme and Murphy, 1980). A statistical analysis of the mean platelet volume of several donors is given in part II of this paper. Because activated platelets and aggregates can assume a wide array of complex shapes having separate shape factors, both were treated as the equivalent spherical particle for the analysis of aggregation. No shape factor was necessary to determine the absolute equivalent sphere volume of these particles.

The use of deep-bore apertures with length-to-diameter ratios of 1.2 considerably reduced the positive skewing of the single platelet log-volume distribution caused by the artifactual overestimation of particle volumes due to the nonuniform electrical and hydrodynamic fields in the sensing zone of the aperture (Grover et al., 1969*a*; Kachel, 1979; Shank et al., 1969; Thom et al., 1969). Indeed, as shown in Table 1, the slight positive skewing of the single platelet log-volume histogram after background subtraction was not sufficient to influence the positive fit of a normal distribution as verified by the Kolmogorov-Smirnov test. This test is easy to perform for continuous frequency distributions and is more powerful than the parametric chi-square test because no assumption is made about the distribution of sampling error. The artifactual positive skewing could be further reduced by using a hydrodynamic focusing device to direct the particle stream through the center of the aperture where the electrical and hydrodynamic fields are more uniform (Kachel et al., 1970; Spielman and Goren, 1968). The deep-bore apertures provided satisfactory results, however, and were more convenient for processing the large number of samples to be counted and sized in the present experiments.

2. Platelet aggregation

A ready index of the degree of aggregation is the decrease in the concentration of single cells. Analysis of the aggregation of platelets from a representative donor revealed a substantial delay before the onset of aggregation at all mean tube shear rates tested and suggested the existence of a limiting shear rate above which aggregation is prevented. Although the rate of aggregation was greatest at $\bar{G} = 168\ s^{-1}$, the collision efficiency, α_o, decreased steadily with increasing mean tube shear rate from $\bar{G} = 41.9$–$1{,}000\ s^{-1}$. Intuitively, this can be understood by realizing that the two-body collision frequency predicted by Eq. 9 for $\bar{G} = 168\ s^{-1}$ was four times that at $\bar{G} = 41.9\ s^{-1}$. Thus, the slope of the curve at $\bar{G} = 168\ s^{-1}$ in Fig. 5 should be four times that at $\bar{G} = 41.9\ s^{-1}$, simply to maintain the same collision efficiency. The inverse relationship between α_o and $\bar{G}$ is in agreement with theory and experiment for suspensions of charged colloidal particles (van de Ven and Mason, 1977). Because the theory is strictly applicable to collisions between single equal-sized spherical particles and assumes no doublet breakup, it is valid only at the early stages of platelet aggregation. As a result, the decrease in α_0 at long mean transit times may simply be due to a lowered collision rate from the

lower particle concentration, despite the greater collision cross-section of the larger particles. Indeed, in the case where aggregation was less extensive, $\bar{G} = 1{,}000\ s^{-1}$, the collision efficiency still appeared to be constant at $\bar{t} = 86$ s. The initiation of aggregation after a delay of $\bar{t} = 21$ s at this shear rate also suggests the presence of more than one type of platelet–platelet bond: an early bond of weak strength and a stronger bond that forms later in time.

Neither changes in the single platelet concentration nor the collision efficiency yielded information on the pattern of aggregate growth or breakup. Because the number concentration of aggregates was so low, the volume fraction of particles was used as an index of aggregate size. Volume fraction histograms revealed that aggregate size increased in discrete increments, even for very large-sized aggregates where the potential variation in size and shape is great. More surprising, at $\bar{G} = 335\ s^{-1}$ there was an initial rapid growth of large aggregates that appeared to break up at longer mean transit times. Thus, the critical shear rate for either the inhibition of aggregation or the initiation of aggregate breakup is likely time-dependent. The large increase in the total volume fraction of particles accompanying the formation of large aggregates of volume between 10^3 and $10^5\ \mu m^3$ is likely the result of an increase in the aggregate void volume (Born and Hume, 1967; Belval and Hellums, 1986), and of the artifactual overestimation of the volume of large particles discussed previously.

Part II is a comprehensive study of the ADP-induced aggregation of human platelets in Poiseuille flow covering many donors. The effects of shear rate, transit time, donor sex, and ADP concentration are followed through the measurement of the single platelet concentration, the collision efficiency, and the volume fraction of particles.

APPENDIX

Details of curve fitting and background subtraction

The fitting of a normal curve to the log-volume histogram $f(x_i)$ and an exponential curve to the background histogram $y(x_i)$ were carried out as follows. A normal curve of the form

$$g(x_i) = f_m e^{-(x_i - \bar{x})^2/2s^2} \tag{A1}$$

was fitted to $f(x_i)$, with f_m the maximum class content of $f(x_i)$, and $\bar{x}$ and s^2 the respective mean and variance of x_i:

$$\bar{x} = \frac{\sum_{i=\ell}^{u} x_i f(x_i)}{\sum_{i=\ell}^{u} f(x_i)}, \tag{A2a}$$

$$s^2 = \frac{\sum_{i=\ell}^{u} f(x_i)(x_i - \bar{x})^2}{\sum_{i=\ell}^{u} f(x_i) - 1}. \tag{A2b}$$

The classes ℓ and u were selected by inspecting $f(x_i)$ and truncating the lower and upper bounds of the single platelet distribution to reduce the effect of background and microaggregate contamination, respectively, on both the initial estimate of $\bar{x}$ and s^2, and the fitting of $g(x_i)$ to $f(x_i)$.

A trial and error iterative procedure minimized the sum of squared errors,

$$E = \sum_{i=\ell}^{u} [f(x_i) - g(x_i)]^2. \tag{A3}$$

Eq. A3 was computed using the initial estimates of f_m, $\bar{x}$, and s^2, which were then successively varied by increments proportional to their magnitude, and E computed again. If E decreased, the newly adjusted parameter replaced the previous parameter. In either case, the increment was decreased by a fractional amount and the procedure repeated until the increment was <1% of the initial increment of each parameter. This was usually the case after 70–80 iterations:

The exponential

$$y'(x_i) = \alpha e^{\beta x_i}, \tag{A4}$$

where α and β are constants, was fitted to the measured background histogram, $y(x_i)$, over the first 50 classes. Expressing Eq. A4 as

$$\ln y'(x_i) = \ln \alpha + \beta x_i \tag{A5}$$

allowed a straight line regression of $\ln y(x_i)$ on x_i. The class contents were weighted in proportion to $y(x_i)$ to counteract the approximate $1/y(x_i)$ weighting which results from using $\ln y(x_i)$ instead of $y(x_i)$ in the regression.

The weighted least squares condition

$$\sum_{i=1}^{50} y(x_i)[\ln y(x_i) - \ln \alpha - \beta x_i]^2 = \text{minimum} \tag{A6}$$

gives rise to the normal equations (Kenney and Keeping, 1951):

$$\ln \alpha \sum_{i=1}^{50} y(x_i) + \beta \sum_{i=1}^{50} x_i y(x_i) = \sum_{i=1}^{50} y(x_i) \ln y(x_i) \tag{A7a}$$

$$\ln \alpha \sum_{i=1}^{50} x_i y(x_i) + \beta \sum_{i=1}^{50} x_i^2 y(x_i) = \sum_{i=1}^{50} x_i y(x_i) \ln y(x_i), \tag{A7b}$$

and hence α and β. Because the background count in PPP was always less than that in the autologous PRP, the magnitude of background was adjusted by the factor $\gamma = [f(x_1) - g(x_1)]/y'(x_1)$, to give the same content in class 1 of the resultant histogram:

$$f^-(x_i) = f(x_i) - \gamma y'(x_i), \tag{A8}$$

as that predicted by $g(x_i)$. A proportionate amount of background was subtracted from the content of each class of $f(x_i)$ at $\bar{t} = 0$ s, and at all subsequent transit times, over the range $x_i = 0$–5 using Eq. A8. The use of Eq. A4 prevented the transfer of random fluctuations in the class contents of $y(x_i)$ due to low particle counts to $f^-(x_i)$ after background subtraction.

Received for publication 15 December 1988 and in final form 22 June 1989.

REFERENCES

Bahr, G. F., and E. Zeitler. 1965. The determination of the dry mass in populations of isolated particles. *Lab. Invest.* 14:955–977.

Bell, D. N. 1988. Physical factors governing the aggregation of human platelets in sheared suspensions. Ph.D. thesis. McGill University, Montreal, Quebec.

Bell, D. N., and H. L. Goldsmith. 1984. Platelet aggregation in Poiseuille flow. II. Effect of shear rate. *Microvasc. Res.* 27:316–330.

Bell, D. N., H. C. Teirlinck, and H. L. Goldsmith. 1984. Platelet aggregation in Poiseuille flow. I. A double infusion technique. *Microvasc. Res.* 27:297–315.

Bell, D. N., S. Spain, and H. L. Goldsmith. 1989*a*. The ADP-induced aggregation of human platelets in flow through tubes. II. Effect of shear rate, donor sex and ADP concentration. *Biophys. J.* 56:829–843.

Bell, D. N., S. Spain, and H. L. Goldsmith. 1989*b*. The effect of red blood cells on the ADP-induced aggregation of human platelets in flow through tubes. *Thromb. Haemostasis.* In press.

Belval, T., and J. D. Hellums. 1986. The analysis of shear-induced platelet aggregation with population balance mathematics. *Biophys. J.* 50:479–487.

Belval, T., J. D. Hellums, and T. Solis. 1984. The kinetics of platelet aggregation induced by shear. *Microvasc. Res.* 28:279–288.

Born, G. V. R. 1962. Aggregation of blood platelets by adenosine diphosphate and its reversal. *Nature (Lond.).* 194:927–929.

Born, G. V. R., and M. Hume. 1967. Effects of the numbers and sizes of platelet aggregates on the optical density of plasma. *Nature (Lond.).* 215:1027–1029.

Brenner, H. 1961. The slow motion of a sphere through a viscous fluid towards a plane surface. *Chem. Eng. Sci.* 16:242–251.

Chang, H. N., and R. Robertson. 1976. Platelet aggregation by laminar shear and Brownian motion. *Ann. Biomed. Eng.* 4:151–183.

Diem, K., editor. 1962. Scientific Tables. Geigy Pharmaceuticals, Montreal, Quebec. 164.

Frojmovic, M. M., M. Newton, and H. L. Goldsmith. 1976. The microrheology of mammalian platelets: studies of rheo-optical transients and flow in tubes. *Microvasc. Res.* 11:203–215.

Gear, A. R. L. 1982. Rapid reactions of platelets studied by a quenched flow approach: aggregation kinetics. *J. Lab. Clin. Med.* 100:866–886.

Gear, A. R. L., and J. K. Lambrecht. 1981. Reduction in single platelets during primary and secondary aggregation. *Thromb. Haemostasis.* 45:298.

Goldsmith, H. L., and S. G. Mason. 1964. The flow of suspensions through tubes. III. Collisions of small uniform spheres. *Proc. R. Soc. A.* 282:569–591.

Goldsmith, H. L., and V. T. Turitto. 1986. Rheological aspects of thrombosis and haemostasis. Basic principles and applications. *Thromb. Haemostasis.* 55:415–435.

Gregg, E. C., and K. D. Steidley. 1965. Electrical counting and sizing of mammalian cells in suspension. *Biophys. J.* 5:393–405.

Grover, N. B., J. Naaman, S. Ben-Sasson, and F. Doljanski. 1969*a*. Electrical sizing of particles in suspensions. I. Theory. *Biophys. J.* 9:1398–1414.

Grover, N. B., J. Naaman, S. Ben-Sasson, F. Doljanski, and E. Nadav. 1969*b*. Electrical sizing of particles in suspensions. II. Experiments with rigid spheres. *Biophys. J.* 9:1415–1425.

Holme, S., and S. Murphy. 1980. Coulter Counter and light transmission studies of platelets exposed to low temperature, ADP, EDTA, and storage at 22°C. *J. Lab. Clin. Med.* 96:480–493.

Hurley, J. 1970. Sizing particles with a Coulter counter. *Biophys. J.* 10:74–79.

Kachel, V. 1979. Electrical resistance pulse sizing (Coulter sizing). *In* Flow Cytometry and Sorting. M. R. Melamed, P. F. Mullaney, and M. L. Mendelsohn, editors. John Wiley & Sons, New York. 61–104.

Kachel, V., H. Metzger, and G. Ruhenstroth-Bauer. 1970. The influence of the particle path on the volume distribution curves according to the Coulter method. *Z. Gesamte Exp. Med.* 153:331–347.

Kenney, J. K., and E. S. Keeping. 1951. Mathematics of Statistics. Part 2. D. van Nostrand, editor. Toronto, Ontario.

Lilliefors, H. W. 1967. On the Kolmogorov-Smirnov test for normality with mean and variance unknown. *Am. Stat. Assoc. J.* 62:399–402.

Manley, R. St. J., and S. G. Mason. 1952. Particle motions in sheared suspensions. II. Collisions of uniform spheres. *J. Colloid Sci.* 7:354–369.

Mundschenk, D. D., D. P. Connelly, J. G. White, and R. D. Brunning. 1976. An improved technique for the electronic measurement of platelet size and shape. *J. Lab. Clin. Med.* 88:310–315.

Nichols, A. R., and H. B. Bosmann. 1979. Platelet aggregation: newly quantified using nonempirical parameters. *Thromb. Haemostasis.* 42:679–693.

Paulus, J. 1975. Platelet size in man. *Blood.* 46:321–336.

Schlichting, H. 1968. Boundary Layer Theory. 6th ed. McGraw-Hill Book Co., New York. 589.

Shank, B. B., R. B. Adams, K. D. Steidley, and J. R. Murphy. 1969. A physical explanation of the bimodal distribution obtained by electronic sizing of erythrocytes. *J. Lab. Clin. Med.* 74:630–641.

Smoluchowski, M. von. 1917. Versuch einer mathematischen Theorie der Koagulationskinetik kolloider Lösungen. *Z. Phys. Chem.* 92:129–168.

Smythe, W. R. 1961. Flow around a sphere in a circular tube. *Phys. Fluids.* 7:756–759.

Smythe, W. R. 1964. Flow around spheroids in a circular tube. *Phys. Fluids.* 7:633–638.

Sokal, R. R., and F. J. Rohlf. 1969. Biometry. Freeman Publications, San Francisco, CA.

Spielman, L., and S. L. Goren. 1968. Improving resolution in Coulter counting by hydrodynamic focusing. *J. Colloid Interface Sci.* 26:175–182.

Swift, D. L., and S. K. Friedlander. 1964. The coagulation of hydrosols by Brownian motion and laminar shear flow. *J. Colloid Sci.* 19:621–647.

Thom, R., A. Hampe, and G. Sauerbrey. 1969. Die elektronische Volumenbestimmung von Blutkörperchen und ihre Fehlerquellen. *Z. Gesamte Exp. Med.* 151:331–349.

van de Ven, T. G. M., and S. G. Mason. 1977. The microrheology of colloidal dispersions. VII. Orthokinetic doublet formation of spheres. *Colloid Polymer Sci.* 255:468–479.

Velick, S., and M. Goren. 1940. The electrical conductivity of suspensions of ellipsoids and its relation to the study of avian erythrocytes. *J. Gen. Physiol.* 23:753–771.

von Behrens, W. E. 1972. Platelet size. Ph.D. thesis. University of Adelaide, Adelaide, South Australia.

Young, I. T. 1977. Proof without prejudice: use of the Kolmogorov-Smirnov test for the analysis of histograms from flow systems and other sources. *J. Histochem. Cytochem.* 25:935–941.